

Numerical equilibria with pressure anisotropy and incompressible plasma rotation parallel to the magnetic field

G. Poulipoulis and G. N. Throumoulopoulos

Section of Astrogeophysics, Physics Department, University of Ioannina, 451 10 Greece

Abstract

It is believed that plasma rotation can affect the transitions to the advanced confinement regimes in tokamaks, such as the High confinement mode (H-mode) and the formation of Internal Transport Barriers. In addition, in order to achieve fusion temperatures modern tokamaks rely on auxiliary heating methods. These methods deposit energy into the charged particles in a specific direction and thus generate significant pressure anisotropy in the plasma. For incompressible rotation with pressure anisotropy the equilibrium is governed by a Generalized Grad-Shafranov (GGS) equation and a decoupled Bernoulli-type equation for the effective pressure, $\bar{p} = (p_{\parallel} + p_{\perp})/2$, where p_{\parallel} (p_{\perp}) is the pressure tensor element parallel (perpendicular) to the magnetic field. In the case of plasma rotation parallel to the magnetic field the GGS equation can be transformed to one equation identical in form with the GS equation. In this study by making use of the aforementioned property of the GGS equation for parallel plasma rotation we constructed numerical equilibria by extending HELENA, an equilibrium fixed-boundary solver. The code solves the GGS equation for a variety of the two free-surface-function terms involved for arbitrary Alfvén Mach number and anisotropy functions. We have constructed ITER-like diverted-boundary equilibria and examined their properties. In particular we examined the impact of rotation and anisotropy on certain equilibrium quantities. The main conclusions are that the addition of pressure anisotropy to rotation allows the profile shaping of the equilibrium quantities in much more extent thus favouring the confinement and allows extension of the parametric space of the Mach number corresponding to higher values. Furthermore, the impact of pressure anisotropy in the equilibrium quantities is stronger than that of the rotation, for all quantities, but the effective pressure. For the pressure components the impact of the pressure anisotropy is the same regardless of whether the power is deposited parallel or perpendicular to the magnetic surfaces, thus implying that there is no preferable heating direction, while for the current density, the heating parallel to the magnetic surfaces seems to be beneficial for the current-gradient driven instabilities.

1 Introduction

In a previous work [1] we extended the equilibrium code HELENA [2] to stationary equilibria with rotation parallel to the magnetic field based on experimental and theoretical evidence that plasma flow has impact on the equilibrium, stability and transport properties of fusion plasmas. Plasma rotation is associated with the appearance of highly peaked density, pressure and temperature profiles, the suppression of some instabilities and the creation of transport barriers either in the H-mode or in discharges with Internal Transport Barriers (see for example [3], [4] and the review papers [5]-[6]). Rotation can be the result of an external source such as electromagnetic power and neutral beam injection used for plasma heating and current drive or can manifest itself (intrinsic flows). It is believed that the reduction of turbulence and the mode decorrelation is the mechanism through which flow affects the confinement. In addition to the flow itself, recent evidence indicates that the spatial variation of the flow affects more strongly the confinement, and thus making plasma rotation a significant ingredient for the exploitation of the future big machines as ITER and later DEMO in which due to the large plasma volume it would be difficult to induce large flow velocities. In these cases it is possible that the intrinsic rotation in these machines can be important [7]. It is proposed that in JET the driving mechanism for the appearance of intrinsic rotation is the pressure gradient [8].

The heating methods used to drive plasma rotation also deposit energy into the charged particles in a specific direction and therefore generate significant pressure anisotropy in the plasma [9, 10, 11, 12, 13], thus modifying the momentum conservation equation and ultimately affecting the equilibrium and stability properties. The magnitude of anisotropy can be significant. Depending on the direction of the energy deposition the pressure component parallel to that direction increases. For example in a MAST NBI discharge the ratio p_{\parallel}/p_{\perp} has been found to be 1.7 [11] and for a JET ICRH discharge the ratio p_{\perp}/p_{\parallel} has been found as high as 2.5 [10], with p_{\parallel} and p_{\perp} the pressure parallel and perpendicular to the magnetic field lines.

Equilibrium is the starting point for stability and transport studies. For axisymmetric systems, as tokamaks, the governing equation is the so-called Grad-Shafranov (GS) equation whose analytic solutions, as the Solovév one, have been found and used for equilibrium and stability studies. These analytic solutions are subject to some limitations which only numerical solutions can lift. To this end, fixed and free boundary equilibrium codes have been developed to solve the equation in realistic situations, i.e. for realistic choices of the boundary (or the currents in the coils for free boundary codes) and for the respective free functions, based on information from experimental data. Specifically here, we refer to the HELENA code, a fixed boundary solver of the GS equation using finite elements, which is used in the present study and further details are given in Sec. 3. In the presence of plasma rotation and pressure anisotropy the equilibrium is governed by a generalised Grad-Shafranov (GGS) equation together with a Bernoulli-type equation involving the effective pressure [14, 15, 16, 17].

From a mathematical point of view, for compressible flows the GGS equation can be either elliptic or hyperbolic. The transition depends on certain critical values of the poloidal velocity. It must be pointed out that due to axisymmetry of the said configurations, the toroidal velocity is inherently incompressible. In the case of compressible flows the GGS equation and the Bernoulli equation are

coupled through the density which, in that case, is not a surface quantity. In the first elliptic region, which is experimentally accessible [18, 19], and many codes have been developed to solve the system of these two coupled equations as DIVA [20, 21], FINESSE [22], FLOW [23], including a version of FLOW that takes into account non-thermal populations [24]. In order to close the system in the aforementioned codes an adiabatic or isothermal equation of state is adopted. These equations of state are associated with either isentropic or isothermal magnetic surfaces, respectively. The problem of equilibrium with anisotropic pressure and toroidal rotation is examined by extension of HELENA [25] or EFIT++ [26]. For the incompressible flow case the consequence is that the density is uniform on the magnetic surfaces, thus the GGS equation (Eq. (9)) becomes elliptic and decouples from the Bernoulli equation. In the case of a fixed boundary, convergence is guaranteed under the requirement of monotonicity for the free functions [27]. A code that also assumes density uniform on magnetic surfaces is TRANSP [28]. Deviations of density on magnetic surfaces have been observed experimentally, thus the use of both compressible in incompressible assumptions in codes contribute in better understanding.

The aim of this work is to develop further the previous work [1] where the fixed boundary equilibrium code HELENA was extended by including incompressible plasma flow parallel to the magnetic field by adding pressure anisotropy and examine the combined effect of rotation and anisotropy on the equilibrium properties. The code is extended taking advantage of the fact that the governing GGS, Eq. (9), under a transformation can be put in a form identical with the static and pressure isotropic well known GS equation.

In the following section the GGS equation for plasmas with incompressible flow and pressure anisotropy is reviewed. In Sec. 3 the HELENA code for parallel flow and pressure anisotropy is presented and the impact of rotation and pressure anisotropy on certain equilibrium quantities is examined on specific constructed equilibria. In Section 4 the main conclusions are presented.

2 Equilibrium equations

The equations governing a magnetically confined plasma with incompressible flow and pressure anisotropy are the following ([29] and ref 6 therein, [16]):

$$\vec{\nabla} \cdot (\rho \vec{v}) = 0 \quad (1)$$

$$\rho(\vec{v} \cdot \vec{\nabla} \vec{v}) + \vec{\nabla} \mathbb{P} = \vec{J} \times \vec{B} \quad (2)$$

$$\vec{\nabla} \times \vec{B} = \mu_0 \vec{J} \quad (3)$$

$$\vec{\nabla} \cdot \vec{B} = 0 \quad (4)$$

$$\vec{\nabla} \times \vec{E} = 0 \quad (5)$$

$$\vec{E} + \vec{v} \times \vec{B} = 0 \quad (6)$$

$$\mathbb{P} = p_{\perp} \mathbb{I} + \frac{\sigma}{\mu_0} |\vec{B}| \quad (7)$$

where ρ is the mass density, \vec{v} the plasma velocity, \mathbb{P} the pressure tensor, \vec{J} the current density, \vec{B} the magnetic field, \vec{E} the electric field, μ_0 the vacuum

permeability and the quantity

$$\sigma = \mu_0 \frac{p_{\parallel} - p_{\perp}}{|\vec{B}|^2} \quad (8)$$

measures the pressure anisotropy with respect to the parallel (p_{\parallel}) and perpendicular (p_{\perp}) to the magnetic surfaces directions.

Assuming an axisymmetric system and defining an effective pressure:

$$\bar{p} = \frac{p_{\parallel} + p_{\perp}}{2}$$

one obtains the following Generalized Grad-Shafranov equation [16]

$$\begin{aligned} (1 - \sigma - M_p^2) \Delta^* \psi + \frac{1}{2} (\sigma - M_p^2)' |\nabla \psi|^2 + \frac{1}{2} \left(\frac{X^2}{1 - \sigma - M_p^2} \right)' \\ + \mu_0 R^2 \bar{p}'_s + \mu_0 \frac{R^4}{2} \left[\frac{\rho(\Phi')^2}{1 - \sigma - M_p^2} \right]' = 0 \end{aligned} \quad (9)$$

Here, $\psi(R, z)$ is the poloidal magnetic flux function associated to the magnetic surfaces, where (R, ϕ, z) are cylindrical coordinates; ϕ is the ignorable coordinate; the function $M_p(\psi)$ is the Alfvén Mach number of the fluid velocity along the poloidal direction; $X(\psi)$ is a surface quantity that refers to the toroidal magnetic field, $B_{\phi} = I/R$. The relation that connects these two quantities is $I = (X - R^2 \sqrt{\rho} M_p \Phi') / (1 - \sigma - M_p^2)$; with $\Phi(\psi)$ being the electrostatic potential. In the static case $\bar{p}_s(\psi)$ coincides with the effective pressure; B is the magnetic field modulus depending on surface quantities and the radial coordinate; $\Delta^* = R^2 \nabla \cdot (\nabla / R^2)$; while derivatives with respect to ψ are denoted by the prime. As mentioned before, a consequence of incompressibility is that the density $\rho(\psi)$ becomes a surface quantity leading to the decoupling of the Bernoulli equation from the GGS (9):

$$\bar{p} = \bar{p}_s(\psi) - \varrho \left(\frac{v^2}{2} - \frac{R^2 (\Phi')^2}{1 - M_p^2} \right) \quad (10)$$

with v being the velocity modulus. The functions $M_p(\psi)$, $\sigma(\psi)$, $X(\psi)$, $p_s(\psi)$, $\rho(\psi)$ and $\Phi(\psi)$ are free. In addition, the parallel and perpendicular components of the pressure tensor are given by:

$$p_{\perp} = \bar{p} - \sigma \frac{B^2}{2\mu_0} \quad (11)$$

$$p_{\parallel} = \bar{p} + \sigma \frac{B^2}{2\mu_0} \quad (12)$$

Details for the derivation of Eq. (9) are given in [16]. The main steps are first to express the divergence free fields (\vec{B} , \vec{J} and $\rho \vec{v}$) in terms of scalar quantities and second, project the momentum equation (2), and Ohm's law, along the toroidal direction, \vec{B} and $\vec{\nabla} \psi$. The projections yield four first integrals in the form of surface quantities and Eqs. (9) and 10.

Applying the transformation [30]

$$u(\psi) = \int_0^{\psi} [1 - \sigma(f) - M_p^2(f)]^{1/2} df \quad (13)$$

to Eq. (9) it becomes

$$\begin{aligned} \Delta^* u + \frac{1}{2} \frac{d}{du} \left(\frac{X^2}{1 - \sigma - M_p^2} \right) + \mu_0 R^2 \frac{d\bar{p}_s}{du} \\ + \mu_0 \frac{R^4}{2} \frac{d}{du} \left[(1 - \sigma) \rho \left(\frac{d\Phi}{du} \right)^2 \right] = 0 \end{aligned} \quad (14)$$

The latter equation does not contain a quadratic term as $|\nabla u|^2$. Once a solution of (14) is obtained, the equilibrium can be completely constructed with calculations in the u -space by employing (13), and the inverse transformation

$$\psi(u) = \int_0^u [1 - \sigma(f) - M_p^2(f)]^{-1/2} df \quad (15)$$

Specifically, the correspondence between u -space and the ψ -space for some quantities are:

$$\bar{p} = \bar{p}_s(u) - \varrho(u) \left[\frac{v^2}{2} - \frac{R^2(1 - \sigma)}{1 - \sigma - M_p^2} \left(\frac{d\Phi(u)}{du} \right)^2 \right] \quad (16)$$

$$\vec{B} = I(\psi) \vec{\nabla} \phi - \vec{\nabla} \phi \times \vec{\nabla} \psi = I(u) \vec{\nabla} \phi - \frac{d\psi}{du} \vec{\nabla} \phi \times \vec{\nabla} u \quad (17)$$

$$\begin{aligned} \vec{J} &= \frac{1}{\mu_0} \left(-\Delta^* \psi \vec{\nabla} \phi + \vec{\nabla} \phi \times \vec{\nabla} I(\psi) \right) = \\ & \frac{d\psi}{du} R^2 \vec{\nabla} \left(\frac{\vec{\nabla} u}{R^2} \right) + \vec{\nabla} u \cdot \vec{\nabla} \frac{d\psi}{du} + \frac{dI(u)}{du} \vec{\nabla} \phi \times \vec{\nabla} u \end{aligned} \quad (18)$$

$$\vec{E} = -\vec{\nabla} \Phi = -\frac{d\Phi(\psi)}{d\psi} \vec{\nabla} \psi = -\frac{d\Phi(u)}{du} \vec{\nabla} u \quad (19)$$

For flows aligned to the magnetic field, ($\Phi' = 0$), Eq. (14) takes the form of the usual GS equation and can be shown that the poloidal, toroidal and total velocity Alfvén Mach numbers are exactly equal; thus we drop the subscript in the Mach number. One additional surface quantity, K , can be obtained by setting

$$\varrho \vec{v} = K \vec{B}, \quad (20)$$

Applying the divergence operator and taking into account the continuity equation, $\vec{\nabla} \cdot (\varrho \vec{v}) = 0$, one obtains $\vec{\nabla} K \cdot \vec{B} = 0$ as was shown in [31]. Finally, the Bernoulli Eq. (10) with the aid of Eq. (20), becomes

$$\bar{p} = \bar{p}_s(\psi) - \frac{1}{2\mu_0} M^2 B^2(\psi, R) = \bar{p}_s(u) - \frac{1}{2\mu_0} M^2 B^2(u, R) \quad (21)$$

3 Numerical equilibria with parallel plasma rotation and pressure anisotropy

In order to examine the impact of parallel plasma rotation in combination with the pressure anisotropy we constructed numerical equilibria by remapping and

making appropriate use of the code HELENA. The code is a fixed boundary equilibrium solver which solves the static GS equation written as:

$$\Delta^* \psi = -F \frac{dF}{d\psi} - \mu_0 R^2 \frac{dP}{d\psi} = -\mu_0 R j_{tor} \quad (22)$$

The code makes use of isoparametric bi-cubic Hermite finite elements to solve the above equation by employing the Galerkin method, which is a non-linear iteration scheme, and using straight-field-line coordinates. The boundary condition consists of specific values for the function ψ on a predefined curve which for the code coincides with the last closed flux surface of its computational domain. The technique has proved to produce high quality results with fast convergence [32].

The following mapping can be established by comparison of Eq. (14) for parallel plasma rotation ($\Phi' = 0$) with Eq. (22):

$$\psi \longleftrightarrow u \quad (23)$$

$$F \frac{dF}{d\psi} \longleftrightarrow \frac{1}{2} \frac{d}{du} \left(\frac{X^2}{1 - \sigma - M^2} \right) \quad (24)$$

$$P(\psi) \longleftrightarrow \bar{p}_s(u) \quad (25)$$

On the basis of this correspondence, it is expected that the use of HELENA for the computation of stationary equilibria for parallel plasma flow and pressure anisotropy is possible, with the following clarification. The solver of the code remains unchanged, but the input/output quantities to it no longer refer to the ψ -space. A correspondence between the ψ -space and the u -space of the input and the calculated by the solver quantities respectively is required. For the minimum set of the basic quantities, the aforementioned mapping is:

$$P_{\text{HELENA}} \longleftrightarrow \bar{p}_s \quad (26)$$

$$F_{\text{HELENA}} \longleftrightarrow \frac{X}{\sqrt{1 - \sigma - M^2}} \quad (27)$$

$$\psi_{\text{HELENA}} \longleftrightarrow u \quad (28)$$

The mapping for the magnetic field, the current density and the pressure by making use of Eqs. (26)-(28) on (17), (18) for $\Phi' = 0$ and (21) is:

$$\vec{B} = \frac{F_{\text{HELENA}}}{\sqrt{1 - \sigma - M^2}} \vec{\nabla} \phi - \frac{1}{\sqrt{1 - \sigma - M^2}} \vec{\nabla} \phi \times \vec{\nabla} u \quad (29)$$

$$\vec{j} = \left[\frac{-1}{\sqrt{1 - \sigma - M^2}} \Delta^* u + \frac{1}{2} \frac{1}{(1 - \sigma - M^2)^{3/2}} \frac{d(\sigma + M^2)}{du} |\vec{\nabla} u|^2 \right] \vec{\nabla} \phi + \frac{d}{du} \left(\frac{F_{\text{HELENA}}}{\sqrt{1 - \sigma - M^2}} \right) \vec{\nabla} \phi \times \vec{\nabla} u \quad (30)$$

$$\bar{p} = P_{\text{HELENA}} - \frac{1}{2\mu_0 R^2} \frac{M^2}{1 - M^2} \left(F_{\text{HELENA}}^2 + |\vec{\nabla} u|^2 \right) \quad (31)$$

where the subscript HELENA refers to the quantities computed by the solver of the Grad-Shafranov equation.

A point of interest is that owing to the fact that the transformation (13) just relabels the magnetic surfaces and that HELENA is a fixed boundary

Table 1: Input values of the basic quantities used for the equilibria solutions.

R_0	$B_{\phi 0}$	I_{plasma}	ψ_{axis}
6.00 m	5.3 T	15.1 MA	0.0 Wb

solver- therefore the “radial” dependence of the magnetic field is not affected by the plasma rotation and pressure anisotropy- the safety factor q is flow and anisotropy independent, as long as the input to the solver remains fixed. One must clarify that the input to the solver is not the same as the input to the code, since the latter depends on the integral transformation, in the presence of rotation and pressure anisotropy. Specifically, the safety factor is given by the relation [33]

$$q(\psi) = \frac{1}{2\pi} \int_0^{2\pi} \left(\frac{rB_\phi}{RB_\theta} \right)_S d\theta = \frac{F(\psi)}{2\pi} \oint \frac{dl_p}{R^2 B_p} = \frac{F(\psi)}{2\pi |\nabla\psi|} \oint \frac{dl_p}{R} \quad (32)$$

The integration in the last two expressions is performed along the curve of a magnetic surface in the poloidal plane and r , θ are cylindrical coordinates of a system with its origin located at the position of the magnetic axis, with $dl_p = \sqrt{(dr)^2 + (rd\theta)^2}$, $B_p = \sqrt{B_r^2 + B_\theta^2} = |\nabla\psi|/R$. Applying the integral transformation on $F(\psi)$ and $\nabla\psi$ and taking into account (29) for the components of the magnetic field we get

$$q(\psi) = q(u) = \frac{F(u)}{2\pi |\nabla u|} \oint \frac{dl_p}{R} \quad (33)$$

Therefore, as long as the input to the solver remains the same, so does the safety factor.

It is worth pointing out that the solutions of (22), and therefore of the extended code, hold for arbitrary functions of the Mach number $M(u)$, anisotropy $\sigma(u)$ and density $\rho(u)$. By varying the input quantities of the modified code we obtained a number of equilibria. As an example, the magnetic surfaces of an ITER-like configuration with input values summarized in Table 1 and input functions for the quantities P and FF' those in Figs. 1 and 2, respectively, are presented in Fig. 3.

In order to calculate all the equilibrium quantities we modelled the free functions $M^2(u)$ and $\sigma(u)$, in two different ways each e.g.,

$$M^2 = M_0^2 (u^m - u_b^m)^n \quad (34)$$

$$M^2 = C \left[\left(\frac{u}{u_b} \right)^m \left(1 - \left(\frac{u}{u_b} \right) \right) \right]^n \quad (35)$$

$$\sigma = \sigma_0 (u^k - u_b^k)^\ell \quad (36)$$

$$\sigma = D \left[\left(\frac{u}{u_b} \right)^k \left(1 - \left(\frac{u}{u_b} \right) \right) \right]^\ell \quad (37)$$

where

$$C = M_0^2 \left(\frac{m+n}{m} \right)^m \left(\frac{n}{m+n} \right)^n$$

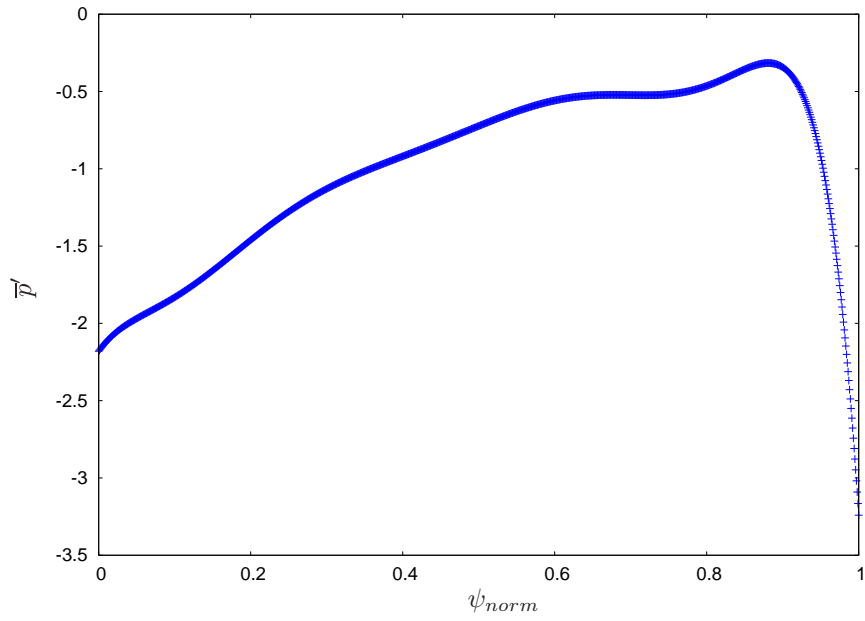


Figure 1: The input profile of the derivative of the effective pressure with respect to a normalized ψ defined as $\psi/\psi_{boundary}$.

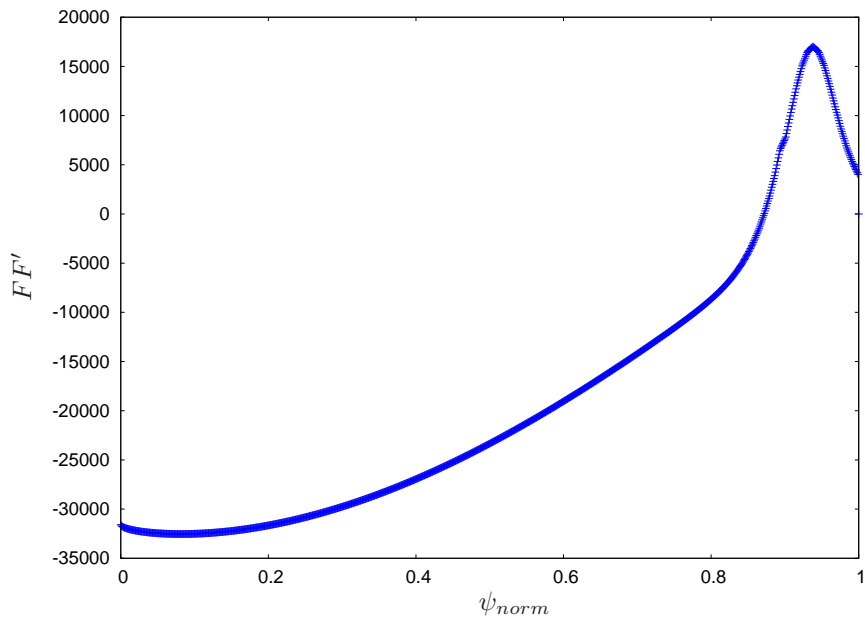


Figure 2: The input profile of FF' used in the runs of the code with respect to normalized ψ .

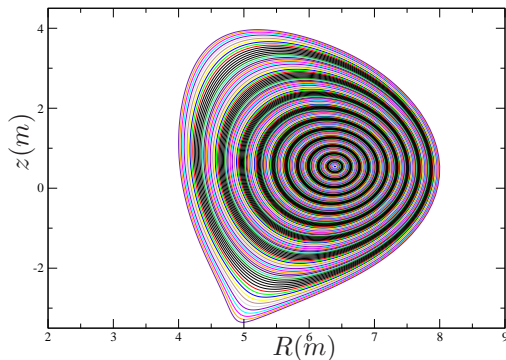


Figure 3: The magnetic surfaces of a diamagnetic equilibrium associated with the values of Table 1 and the input profiles of Figs. 1 and 2. The magnetic axis is located at $(R_a = 6.394 \text{ m}, z_a = 0.54585 \text{ m})$ where the toroidal magnetic field is 4.969 T with respective vacuum value 5.3 T.

and

$$D = \sigma_0 \left(\frac{k + \ell}{k} \right)^k \left(\frac{\ell}{k + \ell} \right)^\ell$$

In this notation, u_b refers to the plasma boundary; the free parameters M_0^2 and σ_0 correspond to the maximum value of M^2 and σ ; and m, n are related to flow shear and the position of the maximum M^2 ; k and ℓ are related to the spatial anisotropy variation (shear) and the position of σ_0 . In particular, (34) and (36) are peaked on- while (35) and (37) peaked off-axis. This specific choice is associated with respective auxiliary heating of tokamaks. For parallel rotation the density does not appear explicitly in the equilibrium equations and hence there is no need to specify it. The scaling $M^2 = \frac{v^2}{B^2/(\mu_0\rho)} \sim \alpha \frac{v_s^2}{B^2/(\mu_0\rho)} \sim \alpha \frac{\gamma P}{B^2/(\mu_0\rho)} \sim \alpha\beta$ where $v_s = (\gamma P/\rho)^{1/2}$ is the sound speed and $\beta = 2P/(B^2/\mu_0)$ can be used to estimate M . Since the maximum experimental value of v in tokamaks is of the order of v_s ($\alpha \sim 0.01 - 0.1$) and $\beta \sim 0.01$, the experimental values of M lie in the interval $(10^{-2}, 10^{-1})$. In small tokamaks where the torque input can produce large plasma flow due to the small volume, the values can be even larger. The choice for peaked on- and off-axis of the Mach number function was motivated by experimental observations of equilibria with plasma rotation [34, 35, 36], while the numerical values of M_0 [37], in some cases well above the experimental values, are used for illustrative reasons. Similarly, the choice for the respective anisotropy profiles is based on physical considerations related to the position where the energy of the heating beams is deposited. In other studies ([13, 11, 12]) the anisotropy was located in the plasma core region. In some cases it is possible to have anisotropy peaked off-axis when the heating is focused in some region away from the magnetic axis. Regarding the values of σ_0 , it is reminded that in JET has been reported anisotropy as high as $p_\perp/p_\parallel \approx 2.5$ [10].

The experimental profiles that are characterized either by a maximum at the magnetic axis or one at a point within the plasma volume was the motivation for the specific choice. At the same time the rotation or the pressure anisotropy are

localized in a finite region of the poloidal plane. However, it should be clarified that the specific choices made for the input profiles do not reproduce precisely experimental profiles throughout the poloidal cross-section. Profile examples for the choices (34) and (35) for M (36) and (37) for σ by varying the free parameters are given in Figs. 4, 5 and 6, respectively.

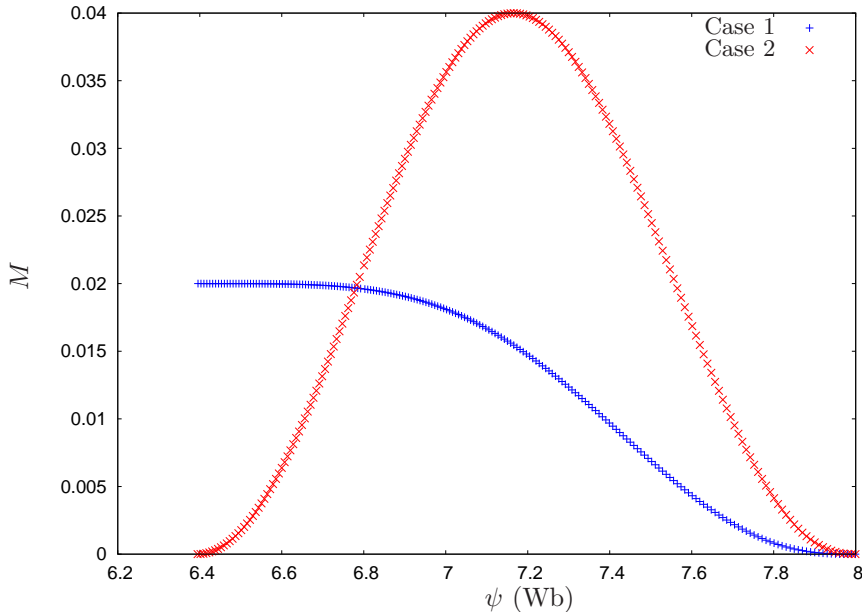


Figure 4: Plots of the Mach number profile with respect to ψ used in the calculated equilibria. Case 1: (blue +) peaked on-axis (Eq. (34)) Mach number with $M_0 = 0.02$, $m = 2$, $n = 3$; Case 2: (red \times) peaked off-axis (Eq. (34)) Mach number with $M_0 = 0.04$, $m = 5$, $n = 2$.

By inspection of Eq. (14) one expects that the rotation has a weak contribution. However, as already mentioned in Sec. 1, it seems that the velocity shear is more important than the velocity amplitude for the transition to improved confinement modes in tokamaks, a result that was reported in [1], in association with equilibrium profiles compatible with ones present in configurations with transport barriers. The impact of pressure anisotropy is expected to be qualitatively the same as the one of the rotation for $\sigma > 0$, though quantitatively it will be stronger than that of the rotation due to the fact that the Mach number enters squared in the equations while σ enters linearly. In addition, the impact of σ on equilibrium differs from that of M because, depending on the energy deposition direction, it can take negative values. The presence of pressure anisotropy allows larger, though out of the experimental limits for the large tokamaks, values for the Mach number. One more point worth noting is that the two free quantities (σ , M) can be potentially used for the shaping of the equilibrium profiles, thus affecting the stability properties of the configuration, especially for gradient-driven instabilities.

We examined the effect of plasma flow and pressure anisotropy in some equilibrium quantities by varying the parameters of the Mach number profile

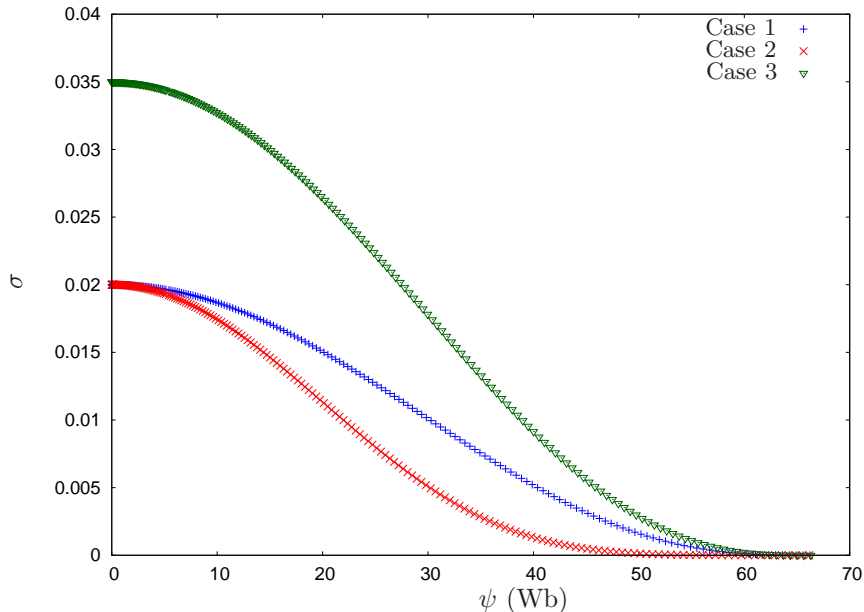


Figure 5: Plots of the on-axis peaked σ profile (Eq. (36)) with respect to ψ for three cases. Case 1: (blue +) $\sigma_0 = 0.02$, $k = 2$, $\ell = 3$; Case 2: (red \times) $\sigma_0 = 0.02$, $k = 2$, $\ell = 6$; Case 3: (green ∇) $\sigma_0 = 0.035$, $k = 2$, $\ell = 3$.

(M_0, n, m) and the pressure anisotropy function (σ_0, k, ℓ) . We note here that any external momentum or energy sources have not been included in the equilibrium equations and therefore the total energy of the system is conserved. Sustaining the configuration after having achieved a desired performance and consequently removing the external energy and momentum sources is desirable for the operation of a tokamak reactor.

A few general remarks regarding the impact of rotation and pressure anisotropy are that the combination of these two quantities allow to shape the equilibrium profiles with great flexibility; specifically, the fact that σ can become negative broadens the region of permissible values for M , thus allowing to access higher plasma rotation velocities. This, in turn, leads to stronger impact of the rotation on those equilibrium quantities where, in addition to the term $(1 - \sigma - M^2)$, there exist other explicit terms of M , M^2 or $(M^2)'$ (cf. Eqs. (14) and (29)-(31)). The impact of plasma rotation and pressure anisotropy with respect to the maximum values as well as to the shear of the profiles of these quantities is examined in detail as it follows. By varying M_0 (or σ_0) on the one hand and n, m (ℓ, k) on the other we examine the impact of plasma rotation (pressure anisotropy) and its shear on the equilibrium. We will focus mainly on the effect of pressure anisotropy and compare it to the one by parallel plasma rotation, while the effect of the latter was individually examined in [1].

By inspection of Eq. (31) is expected that for given p_s , plasma rotation and pressure anisotropy in the case of $\sigma > 0$ reduce the effective pressure values compared to the static and isotropic one (Fig. 7). The fact that now there are two independently varied quantities (M, σ) and one of them can be negative,

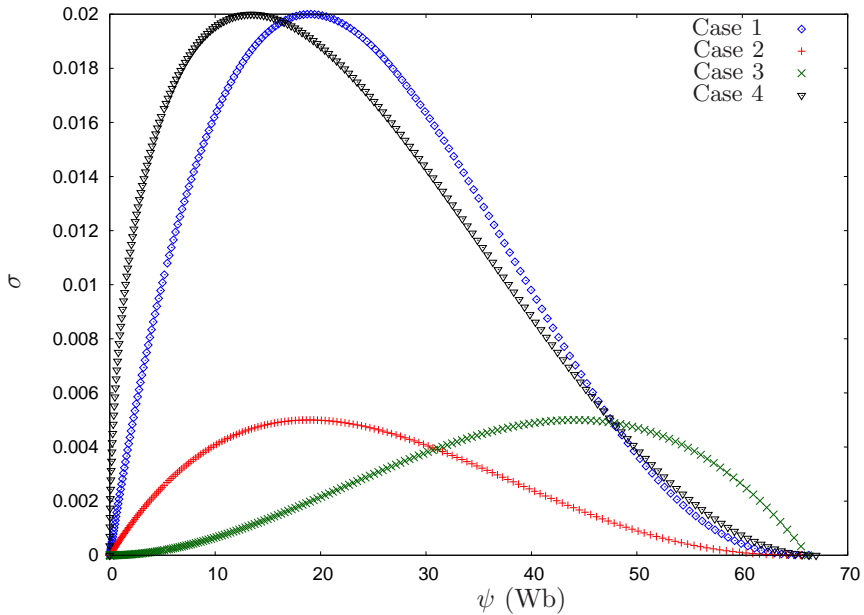


Figure 6: Plots of the off-axis peaked σ profile (Eq. (37)) with respect to ψ for various cases. Case 1: (blue \diamond) $\sigma_0 = 0.02$, $k = 5$, $\ell = 2$; Case 2: (red \times) $\sigma_0 = 0.005$, $k = 5$, $\ell = 2$; Case 3: (green ∇) $\sigma_0 = 0.005$, $k = 2$, $\ell = 4$; Case 4: (black \diamond) $\sigma_0 = 0.02$, $k = 4$, $\ell = 1$.

permits us to shape the profile with great flexibility. It is interesting that the shear of \bar{p} depends more on the maximum value of the pressure anisotropy and less on the values of k and ℓ . It must be noted here that in general the impact of the pressure anisotropy on the effective pressure is negligible. Nevertheless, we present the observed results for completion. As is evident from Figs. 7 and 8 the peaked off-axis profile of the pressure anisotropy affects in greater extent the effective pressure profile compared to the peaked on-axis one. Next, we will focus on the pressure components. It appears that for peaked on-axis σ , the parallel pressure profile flattens on the core, where the maximum value of σ is located, thus helping in reducing pressure-gradient-driven modes while the higher the values of σ_0 , k and ℓ , the larger the shear of the pressure component, in a region within the plasma volume, as is shown in Fig. 9. In addition, the impact of plasma rotation has a weak effect on the components of the pressure as is evident in the same Fig. 9. Pressure profiles with high shear region in the midplane of the poloidal cross-section are observed in discharges with ITBs. As already mentioned above the fact that in the presence of anisotropy, σ can be either positive or negative (see [10], [11]), while it vanishes for isotropic pressure, allows one to explore additional possible experimental configurations, in connection to the direction of the applied heating. The sign of σ appears to affect equally the parallel and perpendicular components of the pressure as it is evident in Figs. 10, 11 and 12, regardless of whether the maximum of σ is located at the magnetic axis or at another point within the plasma volume, thus not favouring a specific set-up. In general, the effect of pressure anisotropy

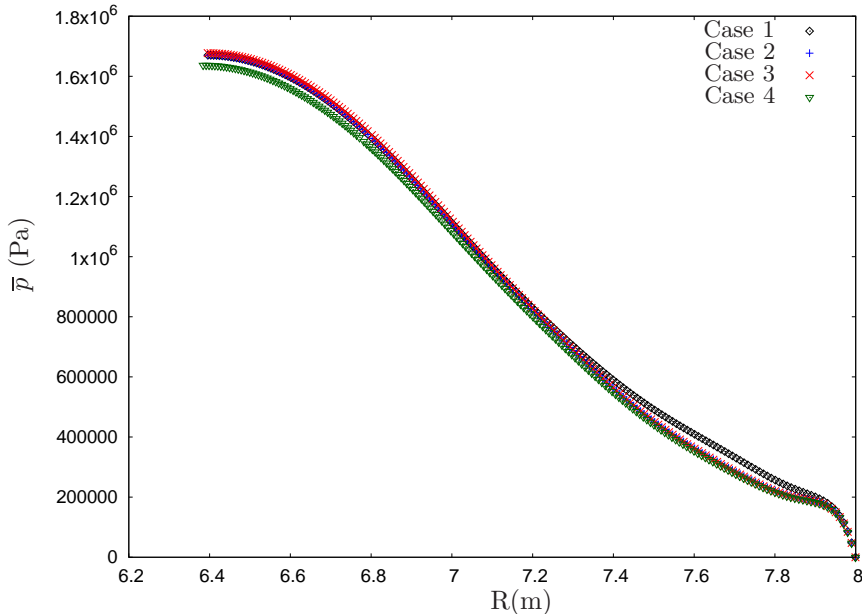


Figure 7: Radial profiles of the effective pressure on the mid-plane $z = 0$ for various cases of pressure anisotropy and plasma rotation. Case 2: (blue $+$) peaked off-axis pressure anisotropy with $\sigma_0 = 0.02$, $k = 5$, $\ell = 2$; Case 3: (red \times) peaked on-axis pressure anisotropy with $\sigma_0 = -0.02$, $k = 5$, $\ell = 2$; Case 4: (green ∇) peaked on-axis pressure anisotropy with $\sigma_0 = 0.02$, $k = 4$, $\ell = 1$. For reference the static effective pressure profile (black \diamond , Case 1) is also given.

on the pressure components is qualitatively the same, though reversed. As is evident from Figures 10 and 12 for $\sigma > 0$ p_{\parallel} increases while p_{\perp} reduces, compared to the isotropic case. The impact of pressure anisotropy appears to be stronger for peaked off-axis σ -profiles compared to cases with peaked on-axis profiles (Figs. 10, 12), a result similar to that for isotropic plasmas with parallel rotation [1]. In the case of isotropic plasmas with parallel rotation the experimental values of M in order to obtain pressure profiles similar to those observed in discharges with ITBs or H-mode plasmas, i.e. profiles with steep regions in the vicinity of the barrier and associated with the maximum of the Mach number profile, appear to be difficult to achieve, especially in large devices. On the contrary, pressure anisotropy which gives similar results for the pressure components profiles is achievable. For peaked off-axis σ -profiles the impact to the pressure components profiles is stronger in the case where the position of σ_0 is closer to the magnetic axis (Fig. 13).

Paying attention to the current density, we must note that for the specific input, the impact on both the parallel and toroidal current density profiles is the same, and therefore we present as examples only of one of the components. The overall conclusion is that the pressure anisotropy can affect the current density much stronger than the parallel rotation. In addition, the impact is localized in the region where the shear of σ is located. Therefore, for peaked on-axis σ -profiles (Fig. 15), the impact on the current density is located towards the

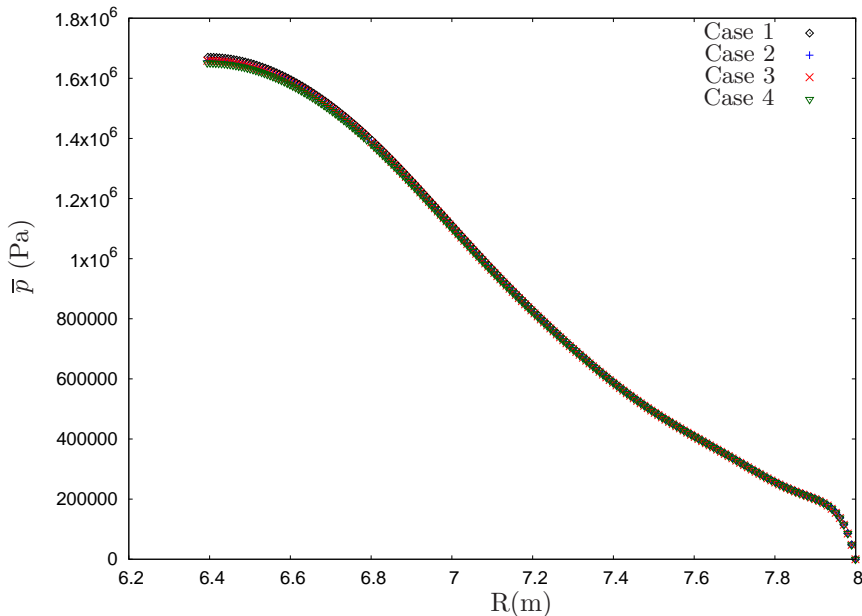


Figure 8: Radial profiles of the effective pressure on the mid-plane $z = 0$ for various cases of pressure anisotropy and plasma rotation. Case 2: (blue $+$) peaked on-axis pressure anisotropy with $\sigma_0 = 0.02$, $k = 2$, $\ell = 3$; Case 3: (red \times) peaked on-axis pressure anisotropy with $\sigma_0 = 0.02$, $k = 2$, $\ell = 6$; Case 4: (green ∇) peaked on-axis pressure anisotropy with $\sigma_0 = 0.035$, $k = 2$, $\ell = 3$. In all cases, the rotation is peaked on-axis with $M_0 = 0.02$, $m = 2$ and $n = 3$. For reference the static effective pressure profile (black \diamond , Case 1) is also given.

edge of the poloidal cross-section, with the extent of this region being dependent on the shape of the σ profile. For peaked off-axis σ -profiles, the current density is affected almost throughout the poloidal cross-section except for the σ_0 point, the boundary and the magnetic axis (Fig. 16). The region of strongest impact is in the middle of the distance between the point of maximum σ and the magnetic axis or the boundary. The above results are similar with the ones obtained in [1] for the impact of parallel rotation on the current density. Compared to the case of parallel rotation, the impact of pressure anisotropy on the current density is apparently more profound, (Figs. 15 and 16). As can be seen from Figs. 17 and 18 for $\sigma < 0$, the current density profiles have increased gradient therefore affecting the relevant modes. Consequently, from the stability point-of-view, it appears that heating parallel to the magnetic surfaces is desirable since it will smooth out the current density profiles. Moreover, the smaller the shear of σ , the smaller the current density gradient. Additionally, regardless of whether it is favourable or not from the stability point-of-view, for peaked on-axis σ -profiles the effect on the current density is stronger for $\sigma < 0$ (Fig. 16) while the opposite is observed for peaked off-axis σ -profiles (Fig. 18).

Regarding the safety factor, though the transformation does not affect its values (cf. Eqs. (32) and (33)), the rotation and the pressure anisotropy alter the q -values through their impact on the input data. Specifically, for $\sigma > 0$, q

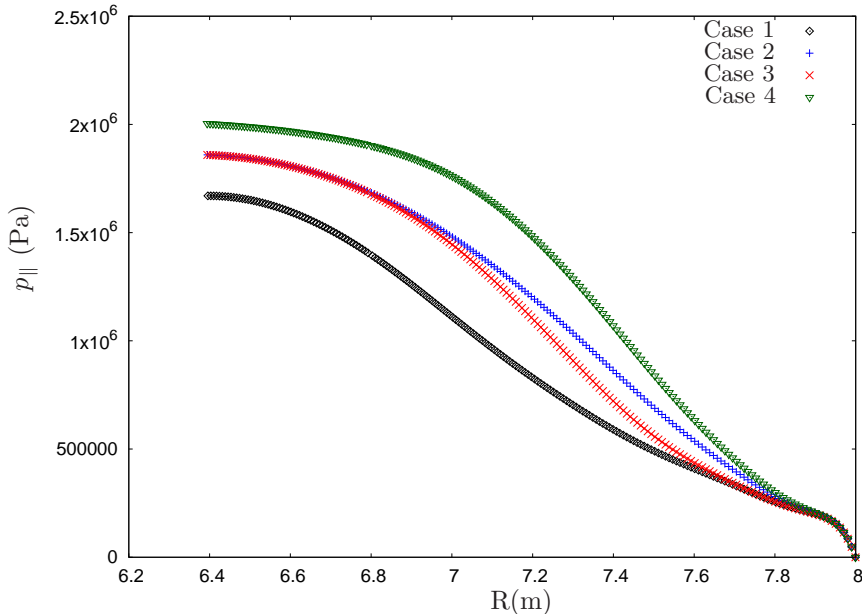


Figure 9: Radial profiles of the parallel pressure on the mid-plane $z = 0$ for various cases of the pressure anisotropy parameters and no plasma rotation. Case 2: (blue +) peaked on-axis pressure anisotropy with $\sigma_0 = 0.02$, $k = 2$, $\ell = 3$; Case 3: (red \times) peaked on-axis pressure anisotropy with $\sigma_0 = 0.02$, $k = 2$, $\ell = 6$; Case 4: (green ∇) peaked on-axis pressure anisotropy with $\sigma_0 = 0.035$, $k = 2$, $\ell = 3$. The static effective pressure (black \diamond , Case 1) is plotted for reference.

increases in the region where the anisotropy is localized. For example, in the case of static anisotropic equilibrium with σ peaked on-axis the values of q at the magnetic axis get larger, as was also reported in [11] while at the boundary either get larger or smaller. For $\sigma < 0$ and peaked on-axis, q decreases thereon. The picture is different for σ -profiles peaked off-axis, i.e. for all the cases examined, the values of q decrease at the magnetic axis as well as at the boundary. As in the case of peaked on-axis σ -profiles, just the opposite occurs for $\sigma < 0$.

Examining the impact of the pressure anisotropy on the position of the magnetic axis, we found an inward shift for peaked on-axis profiles and $\sigma > 0$, a similar result found also in [10], and an outward shift for $\sigma < 0$. For peaked off-axis σ the position remains practically the same. These results regarding the safety factor and the position of the magnetic axis were not observed in [1] due to the weak impact of parallel rotation on these quantities, especially compared to the respective impact of pressure anisotropy. Finally, we examined the impact of pressure anisotropy on the toroidal β , concluding that for positive σ a slight decrease is observed in its values for both peaked on-axis and peaked off-axis profiles for the anisotropy. Note that the toroidal β in the table 2 is defined as

$$\beta_t = \frac{\langle p \rangle}{B_0^2/2\mu_0}, \quad (38)$$

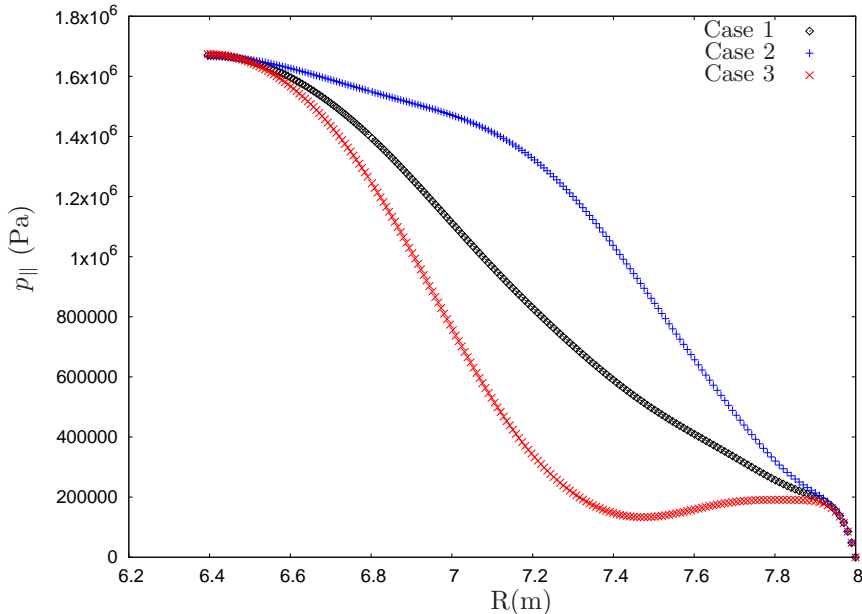


Figure 10: Radial profiles of the parallel pressure on the mid-plane $z = 0$ for various cases of the pressure anisotropy and plasma rotation. Case 2: (blue +) peaked on-axis rotation with $M_0 = 0.02$, $m = 2$, $n = 3$ and peaked off-axis pressure anisotropy with $\sigma_0 = 0.02$, $k = 5$, $\ell = 2$; Case 3: (red \times) peaked on-axis rotation with $M_0 = 0.02$, $m = 2$, $n = 3$ and peaked off-axis pressure anisotropy with $\sigma_0 = -0.02$, $k = 5$, $\ell = 2$. The static effective pressure (black \diamond , Case 1) is plotted for reference.

where

$$\langle p \rangle = \frac{\int_0^{V_0} p dV}{V_0},$$

B_0 the vacuum magnetic field at the geometrical center and V_0 the total plasma volume.

4 Conclusions

We examined the impact of pressure anisotropy and parallel rotation on the equilibrium properties of axisymmetric, toroidally confined plasmas by means of numerically constructed ITER-like configurations. To this end the appropriate GGS equation, with the aid of an integral transformation is put in a form identical to the well-known GS equation. This transformation maps the poloidal flux function ψ to another flux function u preserving the shape of the magnetic surfaces. We modified the fixed boundary equilibrium code HELENA, so that via the direct and the inverse transformation the calculated by the Grad-Shafranov solver equilibrium quantities, now in the u -space, are mapped to the ψ -space.

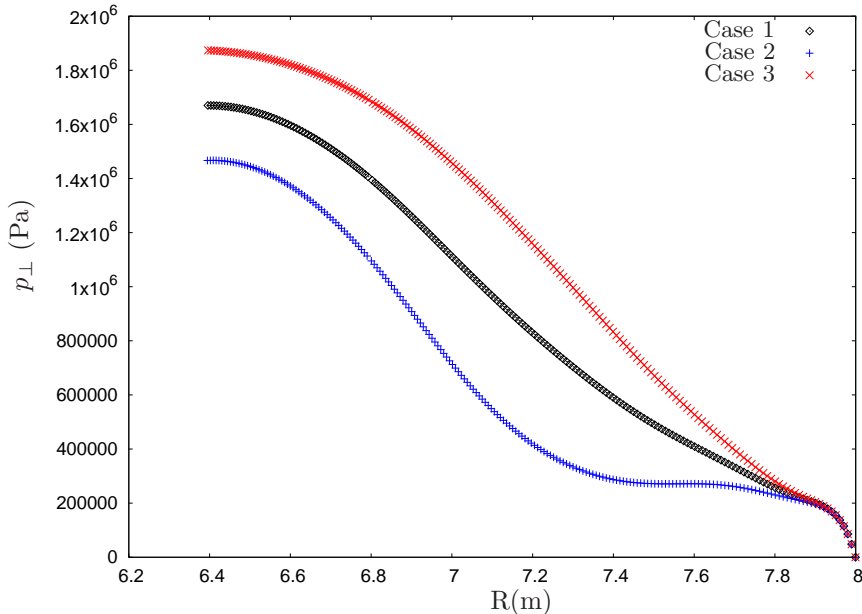


Figure 11: Radial profiles of the perpendicular pressure on the mid-plane $z = 0$ for various cases of the pressure anisotropy and plasma rotation. Case 2: (blue $+$) peaked off-axis rotation with $M_0 = 0.04$, $m = 5$, $n = 2$ and peaked on-axis pressure anisotropy with $\sigma_0 = 0.02$, $k = 2$, $\ell = 3$; Case 3: (red \times) peaked off-axis rotation with $M_0 = 0.04$, $m = 5$, $n = 2$ and peaked on-axis pressure anisotropy with $\sigma_0 = -0.02$, $k = 2$, $\ell = 3$. The static effective pressure (black \diamond , Case 1) is plotted for reference.

On the basis of the equilibria constructed by the code we examined the impact of pressure anisotropy, rotation and their shear on the pressure, toroidal current density, safety factor, position of the magnetic axis and toroidal beta. We mainly focused on the impact of the pressure anisotropy, while the rotation was primarily used for comparison since its impact on the equilibrium was examined in a previous study [1]. The presence of pressure anisotropy in addition to parallel rotation, allows access to configurations with higher values of Mach number, for $\sigma < 0$, and more capabilities in shaping the equilibrium quantities profiles. The effect of pressure anisotropy is much stronger compared to that of parallel rotation on all the quantities we examined, with the exception of the effective pressure. As expected, for $\sigma > 0$ the effective pressure, which enters the GGS equation, is reduced by the pressure anisotropy, though the impact is minimal. The impact on the pressure components of peaked off-axis pressure anisotropy is stronger than that for peaked on-axis anisotropy, and especially for pressure anisotropy localized close to the magnetic axis. In addition, the impact of pressure anisotropy is the same regardless of the sign of σ and also the same for the two pressure components. For the current density the peaked off-axis anisotropy has a stronger impact throughout the poloidal cross-section as opposed to the peaked on-axis case where the impact is localized close to the magnetic axis. This is due to the fact that the shear of pressure anisotropy

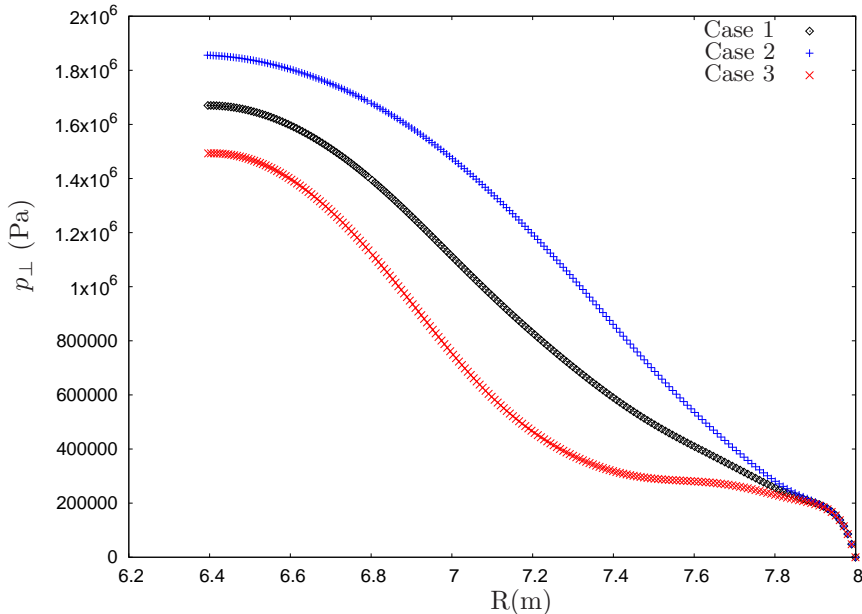


Figure 12: Radial profiles of the perpendicular pressure on the mid-plane $z = 0$ for various cases of the pressure anisotropy and plasma rotation. Case 2: (blue $+$) peaked off-axis rotation with $M_0 = 0.02$, $m = 2$, $n = 3$ and peaked on-axis pressure anisotropy with $\sigma_0 = 0.02$, $k = 2$, $\ell = 3$; Case 3: (red \times) peaked off-axis rotation with $M_0 = 0.02$, $m = 2$, $n = 3$ and peaked on-axis pressure anisotropy with $\sigma_0 = -0.02$, $k = 2$, $\ell = 3$. The static effective pressure (black \diamond , Case 1) is plotted for reference.

has a stronger effect on the current density than the anisotropy itself. In this case that impact is direction independent, unlike the case of parallel rotation which affects more drastically the parallel current component than the toroidal one. The peaked off-axis σ -profile with low shear is smoothing out the current density profiles thus being favourable from the stability point-of-view, since it can affect current-gradient instabilities. It must be noted that, in general $\sigma > 0$ is beneficial for the configuration because it does not produce large current density gradients. For peaked on-axis σ , the safety factor increases at the magnetic axis, while the effect for peaked off-axis profiles is negligible. Also, in certain cases we found that the magnetic axis is shifted inwards for $\sigma > 0$ and outward for $\sigma < 0$. Finally, the toroidal β decreases for $\sigma > 0$ and increases for $\sigma < 0$.

As a next step, it is planned to extend further the computation for non-parallel incompressible plasma rotation. In this case the rotation is associated with electric fields which are believed to play a role in the transitions to improved confinement modes. This can be done on the basis of Eq. (9) (or Eq. (14)) by including the additional electric field dependent R^4 -term therein.

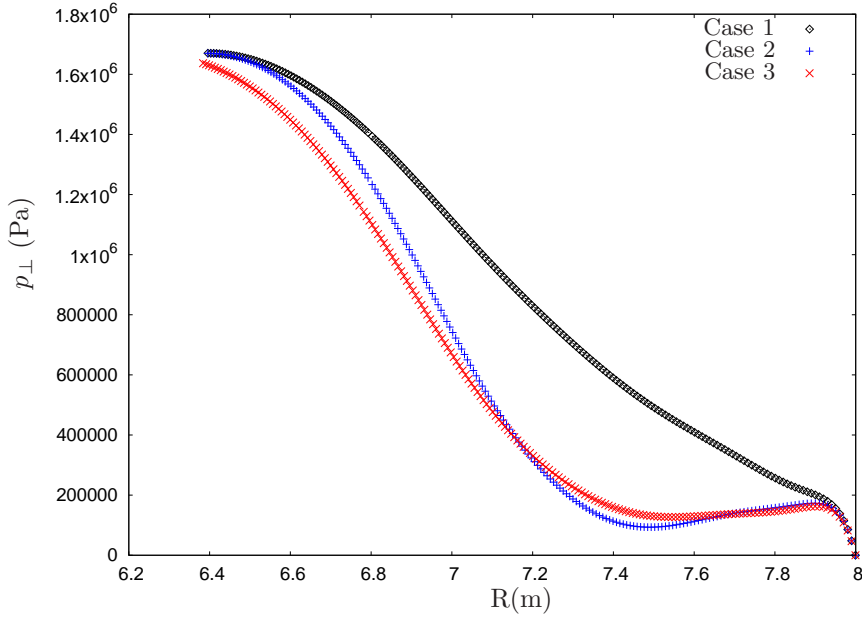


Figure 13: Graphs of the perpendicular pressure components profile in the radial direction at $z = 0$ for various cases of the pressure anisotropy and plasma rotation. Case 2: (blue +) peaked off-axis plasma rotation with $M_0 = 0.04$, $m = 2$, $n = 4$ and peaked off-axis pressure anisotropy with $\sigma_0 = 0.02$, $k = 5$, $\ell = 2$; Case 3: (red \times) rotation as in Case 2 and peaked off-axis pressure anisotropy with $\sigma_0 = 0.02$, $k = 4$, $\ell = 1$. The static effective pressure (black \diamond , Case 1) is plotted for reference.

5 Acknowledgements

This work has been carried out within the framework of the EUROfusion Consortium and has received funding from (a) the Euratom research and training programme 2014-2018 and 2019-2020 under grant agreement No 633053 and (b) the National Program for the Controlled Thermonuclear Fusion, Hellenic Republic. The views and opinions expressed herein do not necessarily reflect those of the European Commission.

References

- [1] G. Poulipoulis, G. N. Throumoulopoulos, and C. Konz. Remapping HELENA to incompressible plasma rotation parallel to the magnetic field. *Physics of Plasmas*, 23(7):072507, July 2016.
- [2] G.T.A. Huysmans, J.P. Goedbloed, and W. Kerner. Isoparametric bicubic Hermite elements for solution of the Grad-Shafranov equation. *International Journal of Modern Physics C*, 2(01):371–376, 1991.
- [3] S. Günter, R.C. Wolf, F. Leuterer, O. Gruber, M. Kaufmann, K. Lackner,

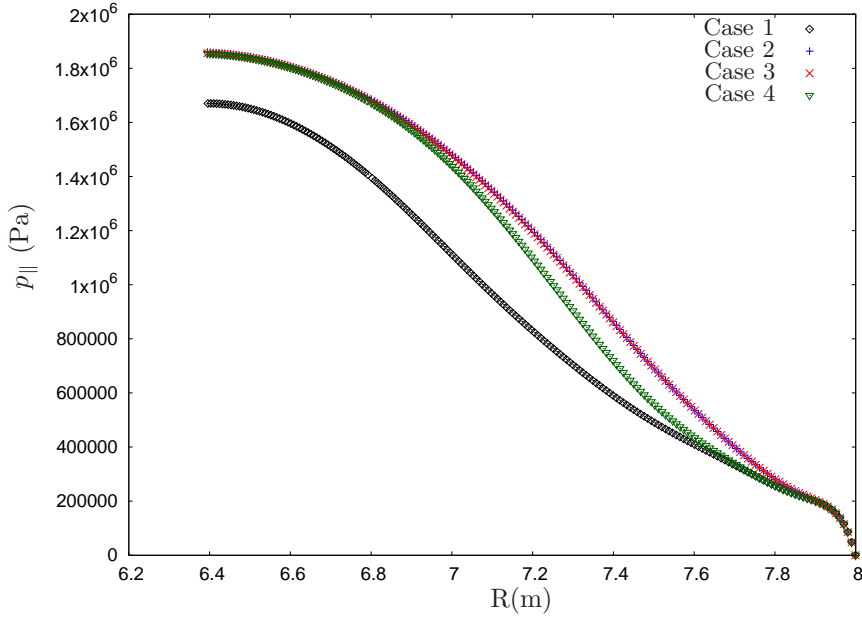


Figure 14: Graphs of the parallel pressure components profile in the radial direction at $z = 0$ for various cases of the pressure anisotropy and plasma rotation. Case 2: (blue +) no rotation and peaked on-axis pressure anisotropy with $\sigma_0 = 0.02$, $k = 2$, $\ell = 3$; Case 3: (red \times) peaked on-axis rotation with $M_0 = 0.02$, $m = 2$, $n = 3$ and peaked on-axis pressure anisotropy with $\sigma_0 = 0.02$, $k = 2$, $\ell = 3$; Case 4: (green ∇) peaked on-axis rotation with $M_0 = 0.02$, $m = 2$, $n = 3$ and peaked on-axis pressure anisotropy with $\sigma_0 = 0.02$, $k = 2$, $\ell = 6$. The static effective pressure (black \diamond , Case 1) is plotted for reference.

M. Maraschek, P.J. Mc Carthy, H. Meister, A. Peeters, G. Pereverzev, H. Salzmann, S. Schade, J. Schweinzer, W. Suttrop, and ASDEX Upgrade the Team. Simultaneous attainment of high electron and ion temperatures in discharges with internal transport barriers in ASDEX upgrade. *Physical Review Letters*, 84(14):3097, 2000.

- [4] F. Romanelli, M. Laxåback, and JET EFDA on behalf of the Contributors. Overview of JET results. *Nuclear Fusion*, 51(9):094008, 2011.
- [5] K. Itoh and S.I. Itoh. The role of the electric field in confinement. *Plasma Physics and Controlled Fusion*, 38(1):1–49, 1996.
- [6] C.D. Challis. The use of internal transport barriers in tokamak plasmas. *Plasma Physics and Controlled Fusion*, 46:B23–B40, December 2004.
- [7] W.M. Solomon, K.H. Burrell, R. Budny, R.J. Groebner, J.E. Kinsey, G.J. Kramer, T.C. Luce, M.A. Makowski, D. Mikkelsen, R. Nazikian, C.C. Petty, P.A. Politzer, S.D. Scott, M.A. Van Zeeland, and M.C. Zarnstorff. Momentum confinement at low torque. *Plasma Physics and Controlled Fusion*, 49(12B):B313, 2007.

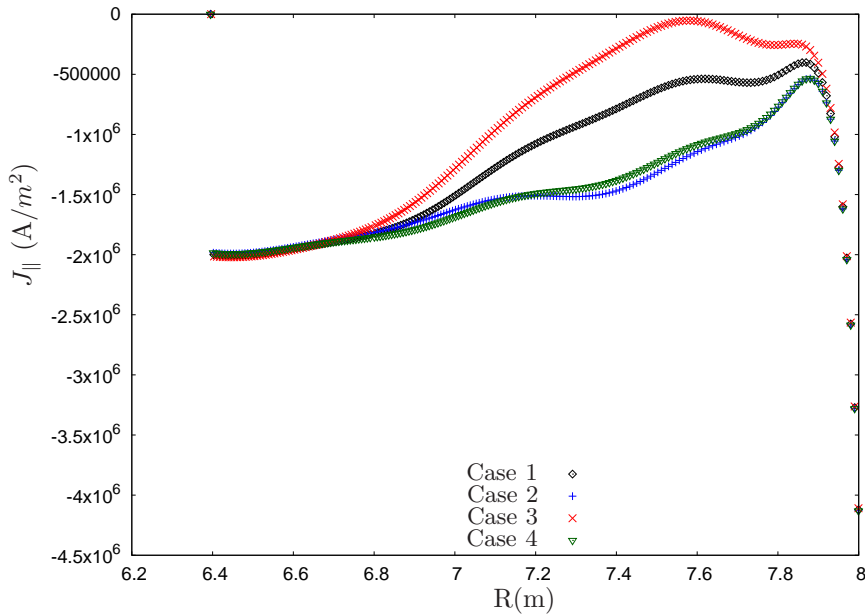


Figure 15: Plots of the parallel to the magnetic field current density versus the radial distance from the axis of symmetry on the mid-plane $z = 0$ for cases of pressure anisotropy peaked on-axis and parallel rotation peaked off-axis. Case 2: (blue $+$) peaked off-axis rotation with $M_0 = 0.04$, $m = 5$, $n = 2$ and peaked on-axis pressure anisotropy with $\sigma_0 = 0.02$, $k = 2$, $\ell = 3$; Case 3: (red \times) peaked off-axis rotation with $M_0 = 0.04$, $m = 5$, $n = 2$ and peaked on-axis pressure anisotropy with $\sigma_0 = -0.02$, $k = 2$, $\ell = 3$; Case 4: (green ∇) no rotation and peaked on-axis pressure anisotropy with $\sigma_0 = 0.02$, $k = 2$, $\ell = 3$. The case of static and isotropic (black \diamond , Case 1) is plotted for reference.

- [8] L.-G. Eriksson, E. Righi, and K.-D. Zastrow. Toroidal rotation in ICRF-heated H-modes on JET. *Plasma Physics and Controlled Fusion*, 39(1):27–42, 1997.
- [9] A. Fasoli, C. Gormenzano, H. L. Berk, B. Breizman, S. Briguglio, D. S. Darrow, N. Gorelenkov, W. W. Heidbrink, A. Jaun, S. V. Konovalov, R. Nazikian, J.-M. Noterdaeme, S. Sharapov, K. Shinohara, D. Testa, K. Tobita, Y. Todo, G. Vlad, and F. Zonca. Chapter 5: Physics of energetic ions. *Nuclear Fusion*, 47:S264–S284, June 2007.
- [10] W. Zwingmann, L.-G. Eriksson, and P. Stubberfield. Equilibrium analysis of tokamak discharges with anisotropic pressure. *Plasma Physics and Controlled Fusion*, 43:1441–1456, November 2001.
- [11] M. J. Hole, G. von Nessi, M. Fitzgerald, K. G. McClements, J. Svensson, and MAST Team. Identifying the impact of rotation, anisotropy, and energetic particle physics in tokamaks. *Plasma Physics and Controlled Fusion*, 53(7):074021, July 2011.

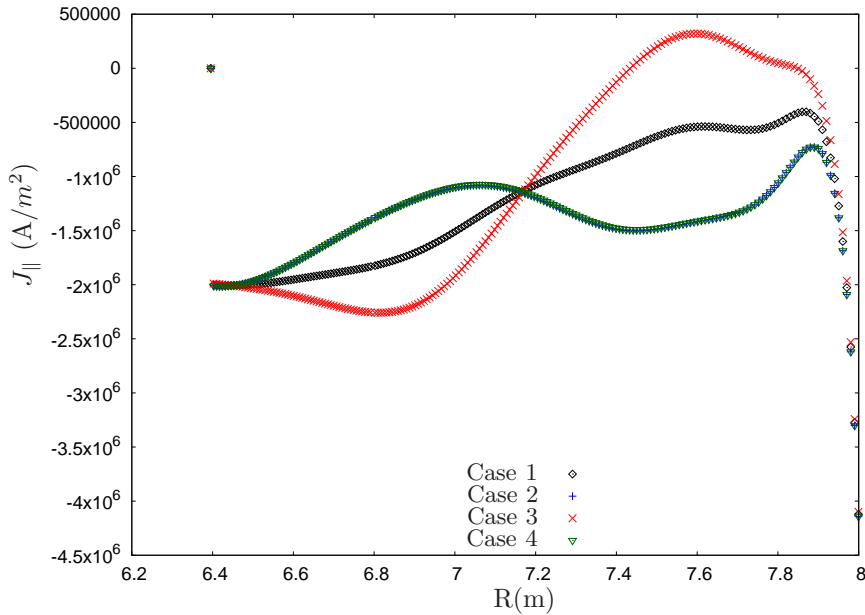


Figure 16: Plots of the parallel to the magnetic field current density versus the radial distance from the axis of symmetry on the mid-plane $z = 0$ for cases of pressure anisotropy peaked off-axis and parallel rotation peaked on-axis. Case 2: (blue $+$) peaked on-axis rotation with $M_0 = 0.02$, $m = 2$, $n = 3$ and peaked off-axis pressure anisotropy with $\sigma_0 = 0.02$, $k = 5$, $\ell = 2$; Case 3: (red \times) peaked on-axis rotation with $M_0 = 0.02$, $m = 2$, $n = 3$ and peaked off-axis pressure anisotropy with $\sigma_0 = -0.02$, $k = 5$, $\ell = 2$; Case 4: (green ∇) no rotation and peaked off-axis pressure anisotropy with $\sigma_0 = 0.02$, $k = 5$, $\ell = 2$. The case of static and isotropic (black \diamond , Case 1) is plotted for reference.

- [12] Zhisong Qu, Michael Fitzgerald, and Matthew John Hole. Analysing the impact of anisotropy pressure on tokamak equilibria. *Plasma Phys. Control. Fusion*, 56:075007, March 2014.
- [13] V. D. Pustovitov. Anisotropic pressure effects on plasma equilibrium in toroidal systems. *Plasma Physics and Controlled Fusion*, 52(6):065001, June 2010.
- [14] A.I. Morozov and L.S. Solov'ev. Steady-state plasma flow in a magnetic field. In *Reviews of Plasma Physics*, pages 1–103. Springer, 1980.
- [15] E. Hameiri. The equilibrium and stability of rotating plasmas. *Physics of Fluids*, 26:230–237, January 1983.
- [16] A. Evangelias and G. N. Throumoulopoulos. Axisymmetric equilibria with pressure anisotropy and plasma flow. *Plasma Physics and Controlled Fusion*, 58(4):045022, April 2016.
- [17] R. A. Clemente and D. Sterzo. Anisotropic ideal magnetohydrodynamic

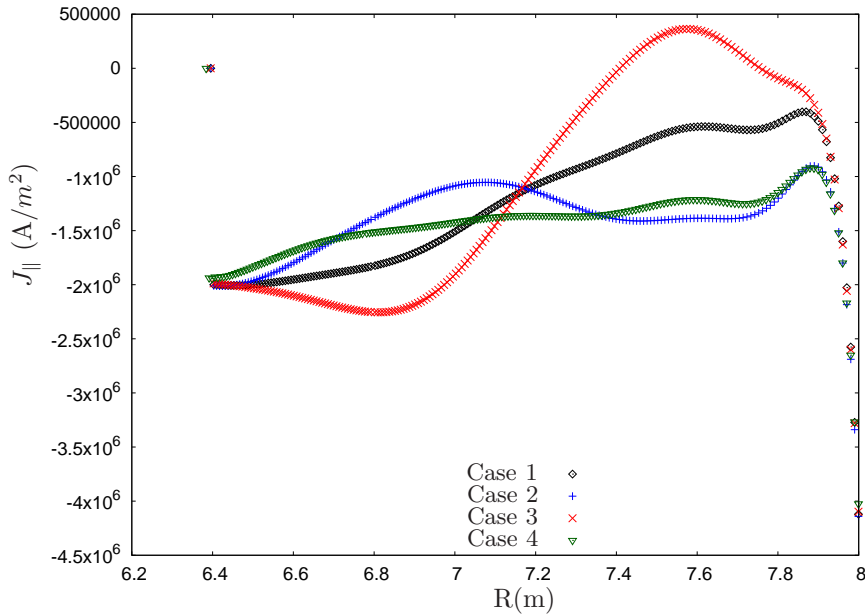


Figure 17: Plots of the parallel to the magnetic field current density versus the radial distance from the axis of symmetry on the mid-plane $z = 0$ for cases of pressure anisotropy peaked on-axis and parallel rotation peaked off-axis. Case 2: (blue $+$) peaked off-axis rotation with $M_0 = 0.04$, $m = 2$, $n = 4$ and peaked off-axis pressure anisotropy with $\sigma_0 = 0.02$, $k = 5$, $\ell = 2$; Case 3: (red \times) peaked off-axis rotation with $M_0 = 0.04$, $m = 2$, $n = 4$ and peaked off-axis pressure anisotropy with $\sigma_0 = -0.02$, $k = 5$, $\ell = 2$; Case 4: (green ∇) peaked off-axis rotation with $M_0 = 0.04$, $m = 2$, $n = 4$ and peaked off-axis pressure anisotropy with $\sigma_0 = 0.02$, $k = 4$, $\ell = 1$. The case of static and isotropic (black \diamond , Case 1) is plotted for reference.

cylindrical equilibria with incompressible adiabatic flow. *Plasma Physics and Controlled Fusion*, 51(8):085011, August 2009.

- [18] For a typical thermonuclear plasma and magnetic field of the order of 1 Tesla, the plasma velocity is of the order of $10 - 10^2$ Km/sec which lies well within the first elliptic region.
- [19] K.G. Mc Clements and M.J. Hole. On steady poloidal and toroidal flows in tokamak plasmas. *Physics of Plasmas (1994-present)*, 17(8):082509, 2010.
- [20] S. Semenzato, R. Gruber, and H.P. Zehrfeld. Computation of symmetric ideal MHD flow equilibria. *Computer Physics Reports*, 1(7):389–425, 1984.
- [21] E. Strumberger, S. Günter, P. Merkel, S. Riondato, E. Schwarz, C. Tichmann, and H.P. Zehrfeld. Numerical MHD stability studies: toroidal rotation, viscosity, resistive walls and current holes. *Nuclear Fusion*, 45(9):1156, 2005.

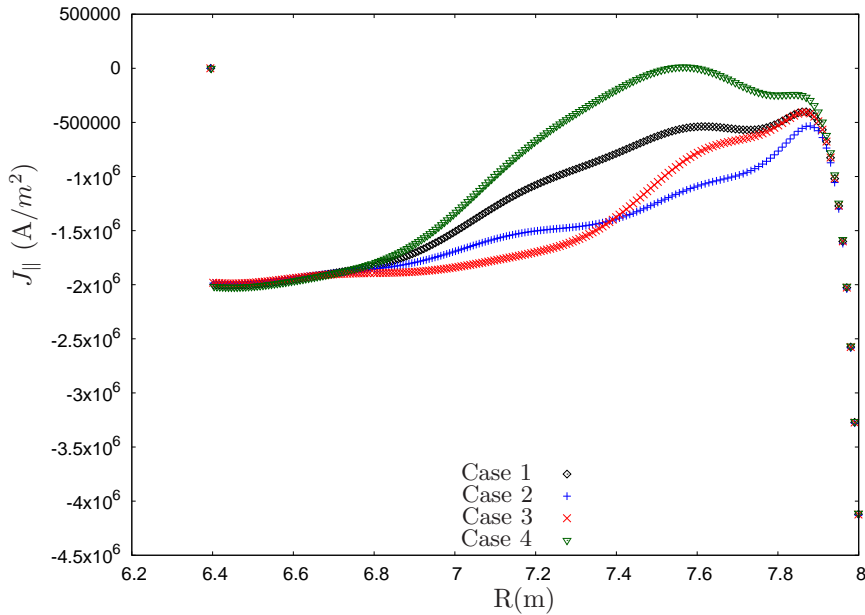


Figure 18: Plots of the parallel to the magnetic field current density versus the radial distance from the axis of symmetry on the mid-plane $z = 0$ for cases of pressure anisotropy peaked off-axis and parallel rotation peaked on-axis. Case 2: (blue $+$) peaked on-axis rotation with $M_0 = 0.02$, $m = 2$, $n = 3$ and peaked on-axis pressure anisotropy with $\sigma_0 = 0.02$, $k = 2$, $\ell = 3$; Case 3: (red \times) peaked on-axis rotation with $M_0 = 0.02$, $m = 2$, $n = 3$ and peaked on-axis pressure anisotropy with $\sigma_0 = 0.02$, $k = 2$, $\ell = 6$; Case 4: (green ∇) no rotation and peaked on-axis pressure anisotropy with $\sigma_0 = -0.02$, $k = 2$, $\ell = 3$. The case of static and isotropic (black \diamond , Case 1) is plotted for reference.

- [22] A.J.C. Beliën, M.A. Botchev, J.P. Goedbloed, B. van der Holst, and R. Keppens. FINESSE: Axisymmetric MHD Equilibria with Flow. *J. Comput. Phys.*, 182(1):91–117, October 2002.
- [23] L. Guazzotto, R. Betti, J. Manickam, and S. Kaye. Numerical study of tokamak equilibria with arbitrary flow. *Physics of Plasmas*, 11(2):604–614, February 2004.
- [24] M.J. Hole and G. Dennis. Energetically resolved multiple-fluid equilibria of tokamak plasmas. *Plasma Physics and Controlled Fusion*, 51(3):035014, March 2009.
- [25] Z.S. Qu, M. Fitzgerald, and M.J. Hole. Analysing the impact of anisotropy pressure on tokamak equilibria. *Plasma Physics and Controlled Fusion*, 56(7):75007–75016, 2014.
- [26] M. Fitzgerald, L.C. Appel, and M.J. Hole. EFIT tokamak equilibria with toroidal flow and anisotropic pressure using the two-temperature guiding-centre plasma. *Nuclear Fusion*, 53(11):113040–113051, 2013.

Table 2: Values of the safety factor and the toroidal β for various cases of rotation and pressure anisotropy.

q	β_t	M_0	m	n	Type	σ_0	k	ℓ	Type
0.6478	0.04199	0	-	-	-	0.02	2	3	on-axis
0.6491	0.04199	0	-	-	-	0.02	2	6	on-axis
0.6517	0.04197	0	-	-	-	0.035	2	6	on-axis
0.6477	0.04199	0.02	2	3	on-axis	0.02	2	3	on-axis
0.6370	0.04204	0	-	-	-	-0.02	2	3	on-axis
0.6387	0.04200	0	-	-	-	0.02	5	2	off-axis
0.6387	0.04200	0	-	-	-	0.02	5	2	off-axis

- [27] R. Courant and D. Hilbert. *Methods of mathematical physics vol. 2*, volume 1. CUP Archive, 1966.
- [28] R.V. Budny, M.G. Bell, A.C. Janos, D.L. Jassby, L.C. Johnson, D.K. Mansfield, D.C. McCune, M.H. Redi, J.F. Schivell, G. Taylor, T.B. Terpstra, M.C. Zarnstorff, and S.J. Zweben. Simulations of alpha parameters in a TFTR DT supershot with high fusion power. *Nuclear Fusion*, 35:1497–1508, 1995.
- [29] D. R. Dobrott and J. L. Johnson. Determination of stellarator equilibria using guiding-center equations. *Plasma Physics*, 11:211–222, March 1969.
- [30] R. A. Clemente. LETTER: Anisotropic axisymmetric equilibria via an analytic method. *Nuclear Fusion*, 33:963–965, June 1993.
- [31] G.N. Throumoulopoulos and H. Tasso. On axisymmetric resistive magnetohydrodynamic equilibria with flow free of Pfirsch-Schlüter diffusion. *Physics of Plasmas*, 10:2382–2388, June 2003.
- [32] C. Konz and R. Zille. *Manual of HELENA Fixed Boundary Equilibrium Solver*. Max-Planck Institute for Plasma Physics, 2007.
- [33] Jeffrey P. Freidberg. *Ideal magnetohydrodynamics*. New York : Plenum Press, 1987., 1987.
- [34] K. Crombé, Y. Andrew, M. Brix, C. Giroud, S. Hacquin, N.C. Hawkes, A. Murari, M.F.F. Nave, J. Ongena, V. Parail, G. Van Oost, I. Voitsekhovitch, and K.D. Zastrow. Poloidal rotation dynamics, radial electric field, and neoclassical theory in the jet internal-transport-barrier region. *Physical review letters*, 95(15):155003, 2005.
- [35] Y. Sakamoto, Y. Kamada, S. Ide, T. Fujita, H. Shirai, T. Takizuka, Y. Koide, T. Fukuda, T. Oikawa, T. Suzuki, K. Shinohara, R. Yoshino, and JT-60 Team. Characteristics of internal transport barriers in JT-60U reversed shear plasmas. *Nuclear Fusion*, 41:865–872, July 2001.
- [36] C.L. Fiore, D.R. Ernst, Y.A. Podpaly, D. Mikkelsen, N.T. Howard, J. Lee, M.L. Reinke, J.E. Rice, J.W. Hughes, Y. Ma, W.L. Rowan, and I. Bespamyatnov. Production of internal transport barriers via self-generated mean flows in Alcator C-Moda). *Physics of Plasmas (1994-present)*, 19(5):056113, 2012.

- [37] P.C. de Vries, M.-D. Hua, D.C. Mc Donald, C. Giroud, M. Janvier, M.F. Johnson, T. Tala, K.-D. Zastrow, and JET EFDA Contributors. Scaling of rotation and momentum confinement in JET plasmas. *Nuclear Fusion*, 48(6):065006, 2008.